Simulations and Localization Accuracy of Image Sensors in their Environment: Theoretical and Monte Carlo Methods

Thomas Cajgfinger

Groupe ebCMOS
Institut de Physique Nucléaire de Lyon
Bâtiment Paul Dirac,
4 rue Enrico Fermi
69622 Villeurbanne

Contents

Introduction

Biological structures span many orders of magnitude in size, but far-field visible light microscopy suffers from limited resolution. A new method for fluorescence imaging [1] has been developed that can obtain spatial distributions of large numbers of fluorescent molecules with a better resolution [2] than the classical diffraction limit ($\sim 200nm$). Fluorescence photoactivation localization microscopy [3, 4] (FPALM) analyzes thousands of single fluorophores per acquisition, localizing small numbers of them at a time, at low excitation intensity. To control the number of visible fluorophores in the field of view and ensure that optically active molecules are separated by much more than the width of the point spread function (psf), photoactivatable fluorescent molecules are used. For these photoactivatable molecules, the activation rate is controlled by the activation illumination intensity; nonfluorescent inactive molecules are activated by a high-frequency (405-nm) laser and are then fluorescent when excited at a lower frequency. The fluorescence is imaged by a CCD camera, and then the molecules are either reversibly inactivated or irreversibly photobleached to remove them from the field of view. The rate of photobleaching is controlled by the intensity of the laser used to excite the fluorescence. Because only a small number of molecules are visible at a given time, their positions can be determined precisely; with only a few detected photons per molecule, the localization precision can be as much as 100-fold better than the resolution [5]. The number of fluorescent molecules and their brightness distribution have also been determined using FPALM. This new method suggests a means to address a significant number of biological questions that had previously been limited by microscope resolution.

Nowadays electronic cameras are used mostly for video applications. With novel technologies, like internet, digital image storage and processing, and new color printing technologies, a whole new branch of applications is being created. Among these are digital still photography, vision and inspection systems, digital video cameras, desktop cameras, scanners and videophones. Consequently, the use of electronic cameras is increasing rapidly. Today, most electronic cameras use CCD-based image sensors. The Charge-Coupled Device or CCD is a well known mature technology. Currently, there is a push in the CCD reserch towards higher resolution, lower pixel dimensions, larger array sizes and less readout noise.

Another type of sensors exists: the Complementary Metal Oxide Semiconductor (CMOS). The origin of the lower image quality of CMOS sensors is the pixel architecture. Various pixel types have been demonstrated in the

past, but the only type which can give comparable noise and sensitivity values as CCDs is the so-called 'active pixel'. This type has an amplification stage in the pixel. In this way, the capacitance on the photodiode node is small, which results in low noise and a high light-to-voltage conversion gain. The drawback of this approach is that the 'fill factor' is low, as a considerable part of the pixel area in consumed by the amplifier transistors and metal lines. As a result, the conversion rate from photons to detected charges is low ($\sim 40\%$). A second disadvantage of the active pixel approach is the pixel non-uniformity due to fixed pattern noise.

The development of detectors tends to smaller pixels and integration time that leads to less photon per pixel per frame. Thus the readout noise should decrease to keep it acceptable for very low light configuration. We need to amplify the photon signal to overcome this readoutnoise. We have two different gain strategies to do so. The first option is the full silicon solution, a gain by impact ionisation into the silicon, like an EMCCD. The second option is a photoconversion and electric field acceleration into a vacuum, like an ebCMOS, as shown in Fig. 1.

It has been shown in previous publications [6] that different sources of noise have an impact on the limit of resolution for a CCD detector. In this work we focused on the differences between the gain processes of these emergent technologies and their associated noises. The pros and cons of the two new generation of single photon detectors are studied with the help of the Cramer-Rao limit and Monte-Carlo simulations. Before that it is important to understand a summary of the different aspects of these detectors.

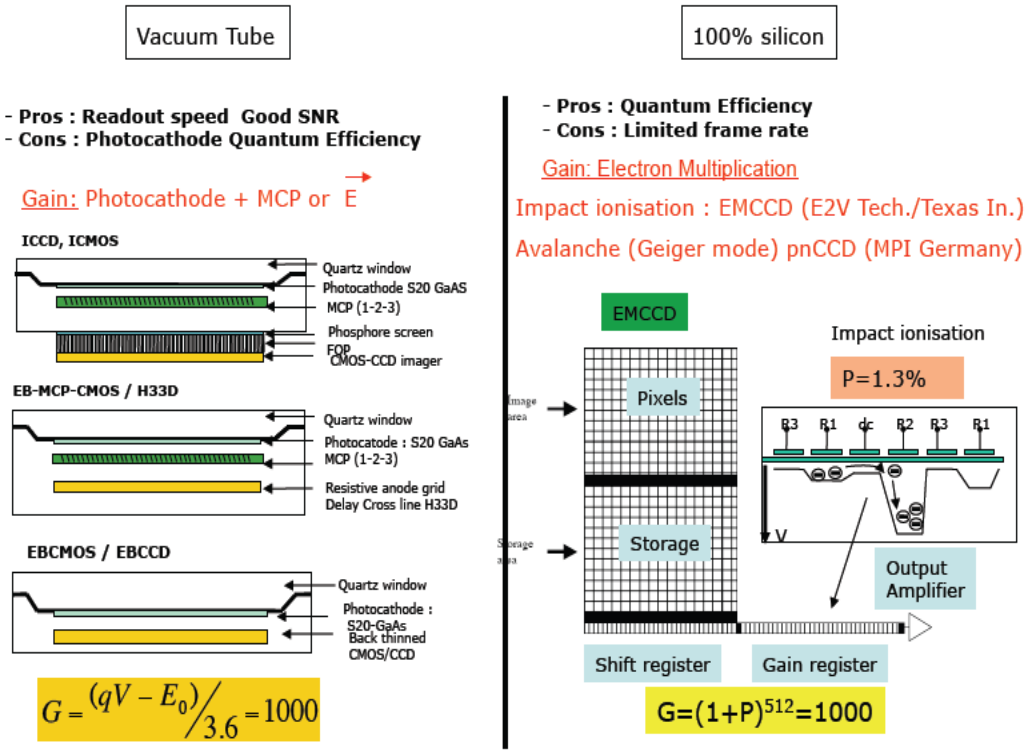

Figure 1: Gain stage options

1 Detectors

1.1 CCD

A charge-coupled device [7] (CCD) is an analog shift register that enables the transportation of analog signals (electric charges) through successive stages (capacitors), controlled by a clock signal. Charge-coupled devices can be used as a form of memory or for delaying samples of analog signals. Today, they are most widely used in arrays of photoelectric light sensors to serialize parallel analog signals.

"CCD" refers to the way the image signal is read out from the chip. Under the control of an external circuit, each capacitor can transfer its electric charge to one or another of its neighbors. CCDs are used in digital photography, digital photogrammetry, astronomy (particularly in photometry), sen-

sors, electron microscopy, medical fluoroscopy, optical and UV spectroscopy, and high speed techniques such as lucky imaging.

1.2 EMCCD

An electron-multiplying CCD [8] (EMCCD, also known as a L3Vision CCD, L3CCD or Impactron CCD) is a CCD in which a gain register is placed between the shift register and the output amplifier. The gain register is split up into a large number of stages. In each stage the electrons are multiplied by impact ionization in a similar way to an avalanche diode. The gain probability at every stage of the register is small (P $<$ 2 %) but as the number of elements is large (N $>$ 500), the overall gain can be very high ($g = (1 + P)^N$) with single input electrons giving many thousands of output electrons. Reading a signal from a CCD gives a noise background, typically a few electrons. In an EMCCD this noise is superimposed on many thousands of electrons rather than a single electron; the devices thus have negligible readout noise.

EMCCDs show a similar sensitivity to Intensified CCDs (ICCDs). However, as with ICCDs, the gain that is applied in the gain register is stochastic [9] and the exact gain that has been applied to a pixel's charge is impossible to know. At high gains (> 30), this uncertainty has the same effect on the signal-to-noise ratio (SNR) as halving the quantum efficiency with respect to operation with a gain of unity [10]. Nevertheless, at very low light levels (where the quantum efficiency is most important) it can be assumed that a pixel either contains an electron - or not. This removes the noise associated with the stochastic multiplication at the cost of counting multiple electrons in the same pixel as a single electron. For multiplication registers with many elements and large gains it is well modeled by the equation [11]:

$$P(n, m, g) = \frac{(n - m + 1)^{m-1}}{(m - 1)!(g - 1 + \frac{1}{m})^m} \exp\left(-\frac{n - m + 1}{g - 1 + \frac{1}{m}}\right), n \geq m \quad (1)$$

where P is the probability of getting n output electrons given m input electrons and a total mean multiplication register gain of g. We plotted this gain for several input electrons in the figure 2.

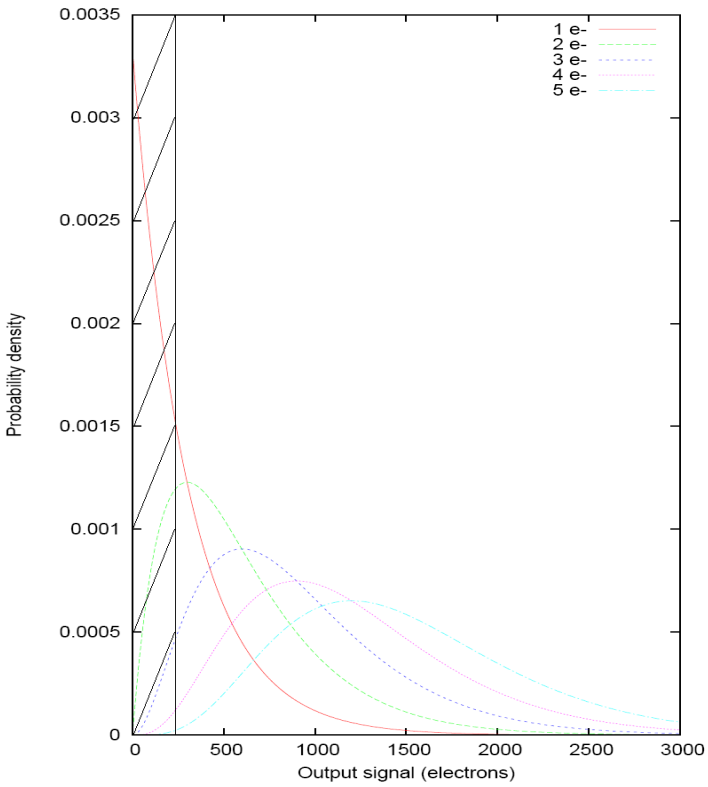

Figure 2: Output signal probability density function of EMCCD with gain 300 obtained with the equation (1)

We note two consequences of the figure 2:

1. the overlaping of the 2,3,4,5 input electrons curves shows that it is impossible to count the number of input electrons.

2. the one input electron curve is very steep around 0. It's a problem in photon counting mode when we cut 5 times the readout noise (hatched area) we can get a 40% effective quantum efficiency (detected photons / incident photons).

1.3 ebCMOS

An ebCMOS, electro-bombarded CMOS, is a new generation of hybrid photo-detectors [12, 13] which associate a back-thinned CMOS sensor with a photo-cathode. The later converts a single photon to a photo-electron which,

in turn, is accelerated in vacuum by an electrostatic field and bombards the back-side of the sensor. Its design is drawn on the Fig. 3.

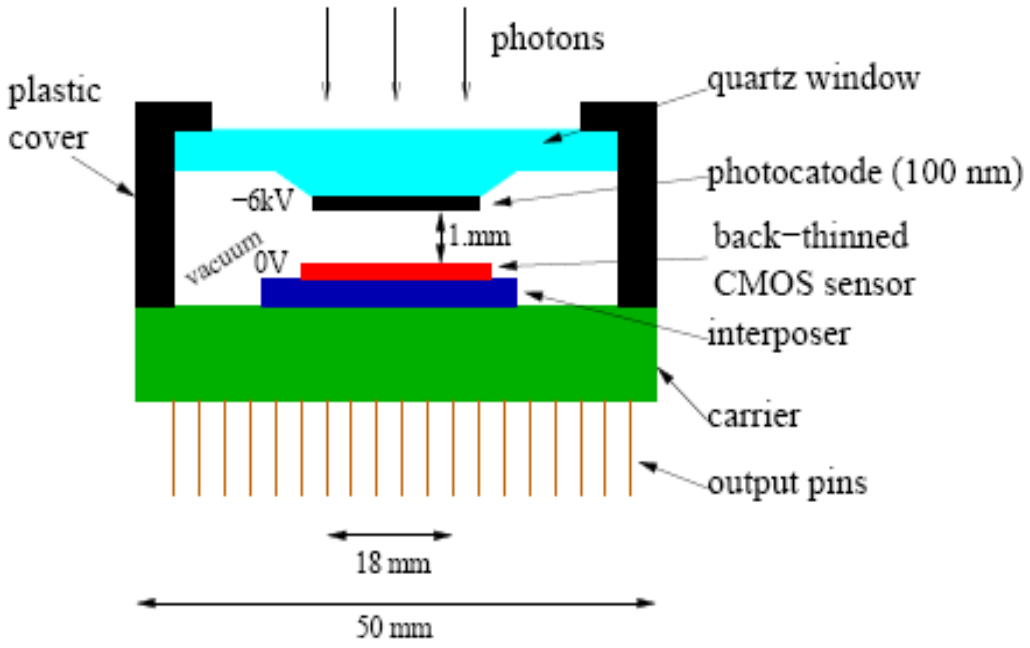

Figure 3: ebCMOS design

The ebCMOS theoretical gain without charge collection efficiency is the number of created electrons for a detected photon:

$$gain = \frac{E - E_{dead}}{\eta} \tag{2}$$

E is the energy of the cathode (typically 4 keV),
E_{dead} is the energy lost in the silicium (typically 1.6 keV),
$\eta = 3.6$ keV is the energy conversion required to create an electron-hole pair.

The main drawback of ebCMOS is its low quantum efficiency (QE). QE is a quantity defined for a photosensitive device as the percentage of photons hitting the photoreactive surface that will produce an electron-hole pair. It is an accurate measurement of the device's electrical sensitivity to light. Since the energy of a photon depends on (more precisely, is inversely proportional

to) its wavelength, QE is often measured over a range of different wavelengths to characterize a device's efficiency at each photon energy.

1.4 Common Noises from Fluorescence Microscopy and Detectors

To simulate the detection process and calculate the localization accuracy, we have to take into account the environment and detector noises.

1.4.1 Scattering Noise

We regrouped in this category the poisson distributed noises [14], which are:

The number of photons that are due to external background radiation in the field of view containing the object of interest (scattering, off-focus photons), also called photon shot-noise.

The number of photons that are due to internal radiation (transistors, diodes, leakage current during integration, reset and readout noises).

1.4.2 Readout Noise

This noise is present in the on-chip amplifier through which all pixel values are read [15]. This is a Gaussian-distributed random variable with a mean of m and a standard deviation of σ. The mean m accounts for a deterministic bias in the amplifier which is distinct from the random, fat-zero bias modeled by the Poisson-distributed Bias noise. In the following, we took m to be 0.

1.5 Specific Noises of the Amplification Processes

With the introduction of gain, we also introduced new noises specific to each amplification strategy (register gain or electric field in vacuum).

1.5.1 Clock Induced Charge (EMCCD)

The first additional component is the spurious noise or Clock Induced Charge (CIC) which originates from within the CCD camera. When charge is shifted pixel to pixel towards the output amplifier there is a very small but finite probability that charges can knock additional charges off by a process called impact ionization. These unwanted charges have the effect of generating an additional noise component. The effect exists in all CCD but in a good camera design the effect is usually minimized and can then only be

seen in exceptional circumstances, for example when binning a very large number of pixels. In a CCD or an ICCD the noise component is so low it is typically hidden by the readout noise or dark current components. In an EMCCD however, spurious charges that occur in the image section are amplified by the EMCCD gain register and therefore are detectable. Incidentally the EMCCD gain register works by effectively harnessing the same effect of impact ionization that creates the spurious charges. The spurious noise can be represented by a charge component that occurs every camera readout cycle. This noise is limited by cooling down the camera to $-80°C$. The CIC effects (background events) for one of the most sensitive EMCCD, ANDOR iXon DU 897BI (512x512 pixels/ $16\mu m$) in photon counting mode are 649 Hz/mm^2 for a gain $g = 1000$ at $T = -85°C$ and 30 ms of frame integration time with 10 MHz readout clock.

1.5.2 Excess Noise Factor (EMCCD)

This noise component originates from the amplification process and is represented by the noise factor. However, the amplification can add noise that must be taken into consideration. It is typically represented by a factor called the noise factor which represents the additional noise over the noise expected from the amplification process. If our camera amplifies our signal by a gain of g we can define our noise factor (F) by the following expression:

$$F^2 = \frac{\sigma_{out}^2}{g^2 \sigma_{in}^2} \tag{3}$$

σ_{in} and σ_{out} are the variances of the input and output signals respectively.The noise factor equals the ratio of the output noise of the amplifier to the input gain g and input noise. An ideal amplifier will therefore have a noise factor of 1. The noise factor for an EMCCD at $g > 300$ is 1.41 [11].

1.5.3 Cathode Dark Current (ebCMOS)

The dark current comes from the cathode due to thermionic or field effects. Typical dark currents obtained at 6 kV and 10°C equals to 650 ± 25 photoelectrons per 27 ms per 2.5 cm^2 for a cathode gap of 1mm. This corresponds to a dark current rate close to 100 Hz/mm^2 [16].

2 Localization Accuracy in Single-Molecule Microscopy

2.1 Fisher Information Matrix and Cramer Rao Lower Bound

The Fisher information [17] is a way of measuring the amount of information that an observable random variable X carries about an unknown parameter θ upon which the likelihood function of θ, $L(\theta) = f(X;\theta)$ depends. The likelihood function is the joint probability of the data, the Xs, conditional on the value of θ, as a function of θ. Since the expectation of the score is zero, the variance is simply the second moment of the score, the derivative of the log of the likelihood function with respect to θ. Hence the Fisher information can be written:

$$I(\theta) = E\left(\left[\frac{\partial}{\partial\theta} ln f(X;\theta)\right]^2 |\theta\right) \tag{4}$$

which implies $0 \leq I(\theta) < \infty$. The Fisher information is thus the expectation of the squared score. A random variable carrying high Fisher information implies that the absolute value of the score is often high. The Fisher information is not a function of a particular observation, as the random variable X has been averaged out. The concept of information is useful when comparing two methods of observing a given random process.

The Cramer-Rao lower bound states that the variance of any unbiased estimator is at least as high as the inverse of the Fisher information. An unbiased estimator which achieves this lower bound is said to be efficient. Such a solution achieves the lowest possible mean squared error among all unbiased methods, and is therefore the minimum variance unbiased (MVU) estimator.

2.2 Fundamental Limit of the Localization Accuracy

Using the Cramer Rao lower bound [18] on the Fisher Information Matrix, we know that for an unbiased estimator θ we have var $(\theta) \geq I^{-1}(\theta)$ where var is the variance and I is the Fisher Information Matrix:

$$I(\theta) = E\left[\left(\frac{\partial L(\theta|z_1 ... z_k)}{\partial\theta}\right)\left(\frac{\partial L(\theta|z_1 ... z_k)}{\partial\theta}\right)^T\right]. \tag{5}$$

E is the expectation value: $E\left[(u(x))\right] = \int_{\Re} u(x)f(x)dx = \int_{\Re} u(x)dF(x)$ where f is a continuous probability density function (pdf) and F the cumulative distribution function: $F(x) = \int_0^x f(x')dx' = P(X < x)$, the Information Matrix is defined by:

$$I(\theta) = \gamma E[N(t)] \begin{pmatrix} \int_{\Re^2} \frac{1}{q(x,y)} \left(\frac{\partial q(x,y)}{\partial x}\right)^2 dxdy & \int_{\Re^2} \frac{1}{q(x,y)} \frac{\partial q(x,y)}{\partial x} \frac{\partial q(x,y)}{\partial y} dxdy \\ \int_{\Re^2} \frac{1}{q(x,y)} \frac{\partial q(x,y)}{\partial x} \frac{\partial q(x,y)}{\partial y} dxdy & \int_{\Re^2} \left(\frac{1}{q(x,y)} \frac{\partial q(x,y)}{\partial y}\right)^2 dxdy \end{pmatrix}$$

Where $N(.)$ is a Poisson counting process with rate A, $E(N(t)] = At$ and γAt is the total number of photons collected by the detector where γ is the optical efficiency.

If the image function q is symmetric for x and y, then $I_{12} = I_{21} = 0$. Therefore the fundamental limit of the localization accuracy, δu on the x-axis, δv on the y-axis, are then $\delta u = \delta v = [I_{11}(\theta)]^{-\frac{1}{2}}$. In what follows, the limit of the localization accuracy is computed for the three devices. The results corresponding to CCD are those obtained in [6]. Those for EMCCD and ebCMOS are original results of this work.

2.3 CCD

The results presented in the following section are those obtained in [6].

2.3.1 Point Spread Function

According to the theory of diffraction, we used a 2D bessel function as a psf to construct likelihood. The probability density function (pdf) $q(x, y)$ that a photon emitted by the source going through the detector arrives at the position (x, y) is:

$$q(x, y) = \frac{J_1^2(\alpha\sqrt{x^2 + y^2})}{\pi(x^2 + y^2)} \tag{6}$$

with $\alpha = \frac{2\pi na}{\lambda}$.

To derive $q(x, y)$ we use the recurrence relation on the Bessel functions:

$$J_n'(r) = \frac{nJ_n(r)}{r} - J_{n+1}'(r) \tag{7}$$

And we get:

$$\frac{\partial q(x,y)}{\partial x} = -\frac{2\alpha x}{\pi}\frac{J_1(\alpha\sqrt{x^2+y^2})}{\sqrt{x^2+y^2}}\frac{J_2(\alpha\sqrt{x^2+y^2})}{x^2+y^2} \tag{8}$$

Then $[I_{11}(\theta)] = [I_{22}(\theta)] = \gamma A t \alpha^2$ and the fundamental limit of the localization accuracy in the noise free without pixelation case is given by:

$$\delta u = \delta v = [I_{11}(\theta)]^{-\frac{1}{2}} = \frac{\lambda}{2\pi n a\sqrt{\gamma A t}} \tag{9}$$

2.3.2 Gaussian Profile

We can approximate the 2D psf by a 2D gaussian function as follow:

$$q(x,y) = \frac{1}{2\pi\sigma_g^2} e^{-\frac{x^2+y^2}{2\sigma_g^2}} \tag{10}$$

And the derivative function:

$$\frac{\partial q(x,y)}{\partial x} = -\frac{x}{\sigma_g} q(x,y) \tag{11}$$

Then $[I_{11}(\theta)] = [I_{22}(\theta)] = \frac{\gamma A t}{\sigma_g^2}$ and the fundamental limit of the localization accuracy is in this case:

$$\delta u = \delta v = \frac{\sigma_g}{\sqrt{\gamma A t}} \tag{12}$$

2.3.3 Effects of Pixelation and Noise

We use a detector with K pixels noted $C_1 ... C_K$. Each pixel is corrupted by poisson noise with mean $b_k t$. And we put an additional readout gaussian noise with mean η_k and variance σ_k^2. The new likelihood is [7, 15]:

$$q_{\theta,k}(z) = \frac{1}{\sqrt{2\pi}\sigma_k} \sum_{l=0}^{\infty} \frac{[\nu_\theta(k)]^l e^{-\nu_\theta(k)}}{l!} e^{-\frac{1}{2}\left(\frac{z-l-\eta_k}{\sigma_k}\right)^2}, z \in \Re \tag{13}$$

with $\nu_\theta(k) = \mu_\theta(k) + b_k t$ where k is the pixel indice and with $\mu_\theta(k) = \gamma A t \int_{C_k} f_\theta$ and $f_\theta = \frac{J_1^2(a\sqrt{x^2+y^2})}{\pi(x^2+y^2)}$.

Using equation(13) we calculate the Fisher information matrix elements:

$$[I(\theta)]_{ij} = \sum_{k=1}^{K} \frac{\partial \mu_\theta(k)}{\partial \theta_i} \frac{\partial \mu_\theta(k)}{\partial \theta_j} \Psi(k) \tag{14}$$

with

$$\Psi(k) = \int_{\Re} \frac{1}{q(k)} \left(\frac{\partial q}{\partial \mu}(k) \right)^2 = \frac{e^{-\nu_{\theta(k)}}}{\sqrt{2\pi}\sigma_k} \int_{\Re} \frac{\left(\sum_{n=1}^{\infty} \frac{(\nu_\theta(k))^{n-1}}{(n-1)!} e^{-\frac{1}{2\sigma_k^2}(z-\eta k-n)^2} \right)^2}{\sum_{n=0}^{\infty} \frac{(\nu_\theta(k))^n}{(n)!} e^{-\frac{1}{2\sigma_k^2}(z-\eta k-n)^2}} dz - 1 \tag{15}$$

Using $J_1'(x) = \frac{J_1(x)}{x} - J_2(x)$ and that $\frac{\partial \mu_\theta(k)}{\partial \theta} = \gamma A t \int_{C_k} \frac{\partial f_\theta}{\partial \theta}$ we find:

$$[I(\theta)]_{11} = \sum_{k=1}^{K} 2\gamma t \alpha^2 \mathcal{J}_x^2 \Psi(k) \tag{16}$$

$$[I(\theta)]_{22} = \sum_{k=1}^{K} 2\gamma t \alpha^2 \mathcal{J}_y^2 \Psi(k) \tag{17}$$

$$[I(\theta)]_{12} = [I(\theta)]_{21} = \sum_{k=1}^{K} 2\gamma t \alpha^2 \mathcal{J}_x \mathcal{J}_y \Psi(k) \tag{18}$$

where

$$\mathcal{J}_x(k) = \int_{C_k} (x - Mu) \frac{J_1(a||r - r_0||)}{\pi ||r - r_0||} \frac{J_2(a||r - r_0||)}{||r - r_0||^2} dr \tag{19}$$

$$\mathcal{J}_y(k) = \int_{C_k} (y - Mv) \frac{J_1(a||r - r_0||)}{\pi ||r - r_0||} \frac{J_2(a||r - r_0||)}{||r - r_0||^2} dr \tag{20}$$

Finally, with $I^{-1} = \frac{1}{det(I)} \begin{pmatrix} I_{22} & I_{21} \\ I_{12} & I_{11} \end{pmatrix}$ we find:

$$I_{11}^{-\frac{1}{2}} = \delta u \left(\frac{1}{2\sqrt{\gamma A t}} \left[\sum_{k=1}^{K} \mathcal{J}_x^2(k) \Psi(k) - \frac{\left(\sum_{k=1}^{K} \mathcal{J}_x \mathcal{J}_y(k) \Psi(k) \right)^2}{\sum_{k=1}^{K} \mathcal{J}_y^2(k) \Psi(k)} \right]^{-\frac{1}{2}} \right) \tag{21}$$

2.4 EMCCD

We have to include the gain given by equation (1) into the CCD likelihood function given by equation (13) where $\nu_\theta(k) = \mu_\theta(k) + b_k t$ is in this case the number of electrons going through the gain process. Thus the number of output electrons is then n with the probability $P(n, \nu_\theta(k), g)$ and the likelihood function becomes:

$$q_{\theta,k}(z) = \frac{1}{\sqrt{2\pi}\sigma_k} \sum_{l=0}^{\infty} \sum_{i=0}^{\infty} \frac{i^l}{l!} e^{-i} e^{-\frac{1}{2}\left(\frac{z-l-\eta_k}{\sigma_k}\right)^2} P(n, \nu_\theta(k), g), z \in \Re \tag{22}$$

The θ dependence is now only on P. Then we have:

$$\frac{\partial q_{\theta,k}(z)}{\partial \theta} = \frac{1}{\sqrt{2\pi}\sigma_k} \sum_{l=0}^{\infty} \sum_{i=0}^{\infty} \frac{i^l}{l!} e^{-i} e^{-\frac{1}{2}\left(\frac{z-l-\eta_k}{\sigma_k}\right)^2} \frac{\partial P(n, \nu_\theta(k), g)}{\partial \mu_{\theta,k}} \frac{\partial \mu_{\theta,k}(z)}{\partial \theta}, z \in \Re \tag{23}$$

The equation using the same results as in equation (21) with a new Ψ defined as in equation (15) has been carefully numerically coded, using a Gauss-Legendre numerical integration at 64 points, and taking into account the numerical infinity problems.

2.5 ebCMOS

We used the Gauss approximation for the ebCMOS detector because it has a multiplying stage with a tube and an acceleration stage that affects the variance of the function. Moreover, the gain stage is linear thus the number of detected photons is amplificated by the gain factor. We got $\sigma_{tot}^2 = \sigma_{opt}^2 + \sigma_{tube}^2 + \sigma_{cmos}^2$ where σ_{opt} and σ_{tube} are spatial pdf and σ_{cmos} is due to the gain process into the silicon. The number of collected electrons becomes $\frac{E-E_{dead}}{3.6} \sum_{k=1}^{K} \mu_\theta(k)$ where $\mu_\theta(k)$ is the number of photons collected by the pixel k.

3 Monte Carlo

3.1 Synoptic of the pdf and Amplification Strategies

In Fig. 4 is drawn a summary of the path followed by photons emitted by a point source and going through a detector used to compute the Monte Carlo

simulation.

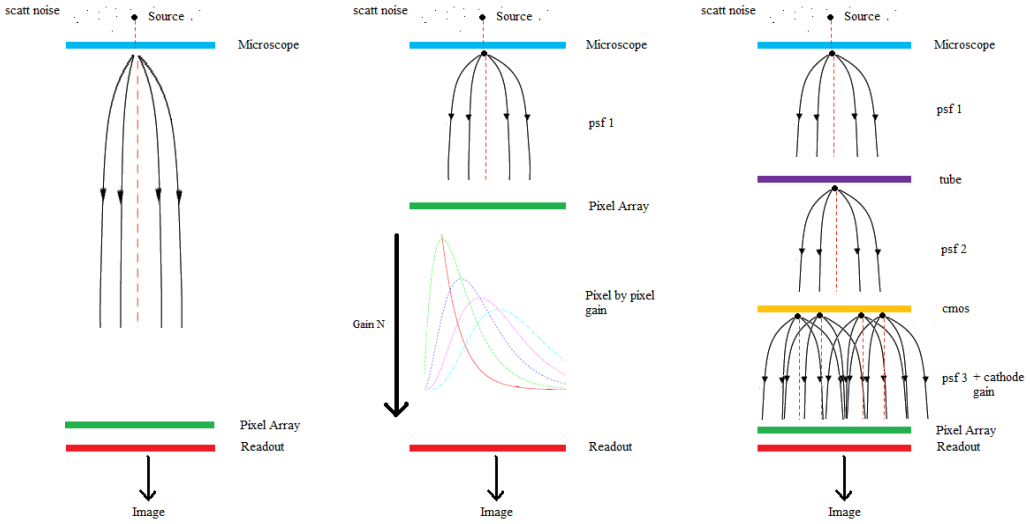

Figure 4: CCD (left),EMCCD (center) and ebCMOS (right)

We can easily see the difference between the two gain stages. For the EMCCD it's a pixel by pixel gain and for the ebCMOS the gain spreads on multiple pixels.

3.2 Events Display

In Fig. 5,6 and 7 are shown samples of Monte Carlo events. We can observe any abnormality and the difference of behavior of detectors when we reduce the signal to few photons.

3.2.1 CCD

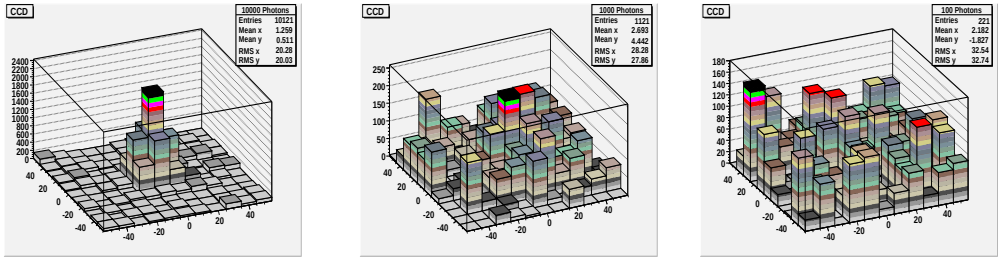

Figure 5: One Frame using CCD detector for 10000 (left),1000 (middle) and 100 (right) photons.

We can easily see the effect of readout noise when the number of detected photons decrease to values lower than 1000.

3.2.2 EMCCD

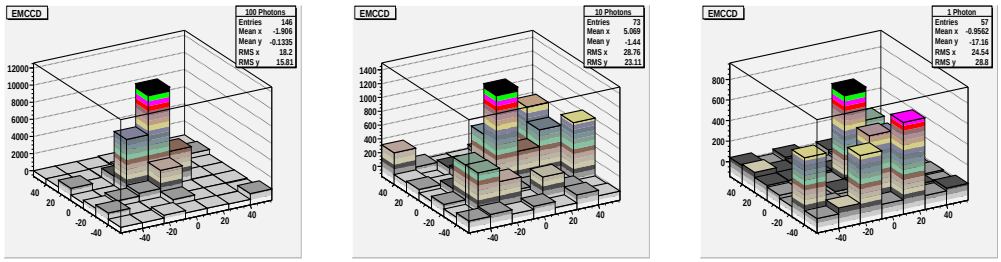

Figure 6: One Frame using EMCCD detector for 100 (left),10 (middle) and 1 (right) photons.

In these frames we can see the advantage of the gain process with the disappearance of the readoutnoise. We can also see its drawback at low detected photons where we cannot distinguish the source and the various shot noises because of the stochastic nature of the amplification.

3.2.3 ebCMOS

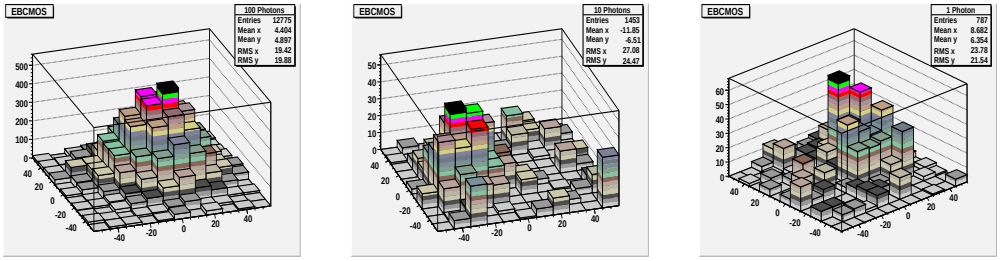

Figure 7: One Frame using ebCMOS detector for 100 (left),10 (middle) and 1 (right) photons.

The ebCMOS has a linear gain stage thus this problem is not relevant here but we can see that because of the widening of the pdf, we have a imprecision about the position of one detected photon.

3.3 Fitting Method

We use the log-likelihood fit with the framework Root using a gaussian function. We sampled 300 images and calculated the root mean square (rms) of the results of the maximum likelihood (ML) minimization and compared it with the limit of the localization accuracy.

4 Results

4.1 Settings

In the following the value of every parameter is as listed in the tables 1,2 and 3 except when indicated.
The values of the common parameters used in both these simulations are summarized in the table 1.

Table 1: Common parameters for Monte Carlo simulation and Cramer Rao limit

σ_{opt}	Scattering Noise	Optical Efficiency	λ (nm)	n_a	M
$8\mu m$	660 photons/pixel/s	0.033	520	1.4	100

The values of the specific parameters used in both these simulations are summarized in the table 2.

Table 2: Specific parameters for Monte Carlo simulation and Cramer Rao limit

Parameters	CCD	ebCMOS	EMCCD
Pixel Array Size	11x11	11x11	7x7
Pixel Dimensions (μm)	10	10	16
Readout Noise (e-/pixel)	57	10	30
Acquisition time (ms)	50	2	30
Quantum efficiency	0.80	0.15	0.80

Moreover we took a gain $g = 300$ for the EMCCD and the ebCMOS settings are in the table 3.

Table 3: ebCMOS parameters

Gain	E_{dead}	σ_{tube}	σ_{cmos}
4 kV	1.6 keV	15 μm	11 μm

4.2 Code Validation

4.2.1 Cramer Rao Lower Bound

We compared the results of the CCD part of our code with [6]. We found the same results but we decided to use the gaussian approximation of the Airy function to compare the results with the Monte Carlo simulations. For the EMCCD and ebCMOS we had no point of comparison but the results were in the expected range.

4.2.2 Monte Carlo

We also compared the results of the Monte Carlo simulations and we found the same ratio between the results and the same order of magnitude but with a difference nonetheless. We assumed that difference came from the fitting method. Our method was quite simple and could have been improved but that was not the goal of this work. This will be looked at in a future work but still allows a comparative study.

4.3 Overview

We use the theoretical limit of Cramer Crao and the Monte Carlo simulation in order to compare the three detectors in differents settings. First we wanted to see the behavior of these detectors when we changed some parameters to understand their strenghs and weaknesses depending on noise conditions of imaging.

4.3.1 SNR

First we can look at the signal to noise ratio (SNR) variations for the three devices to see their behavior when we increase the scattering noise. In Fig. 8 the variation of the ML (rms) is plotted as a function of the SNR for the three types of devices and for different number of detected photons.

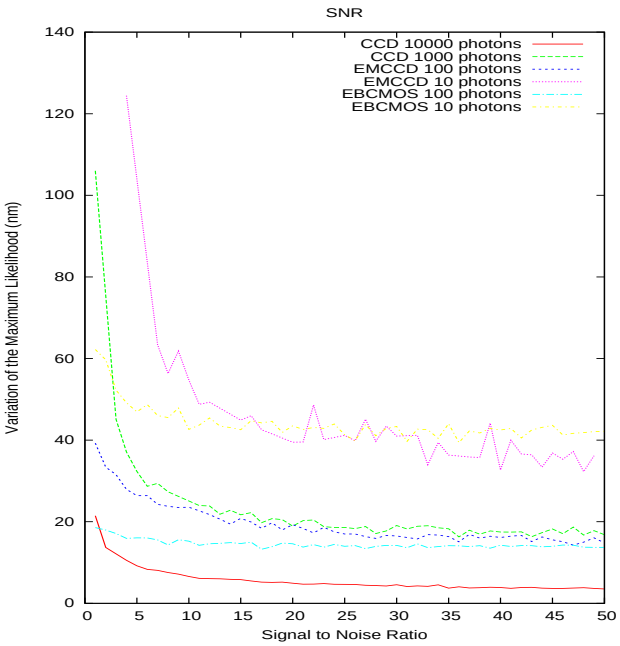

Figure 8: Signal to Noise Ratio Variations

The first thing we can notice is that the both gain processes allow us to divide the number of required detected photons by a factor 10 to 100 for the same accuracy. After that we see that the EMCCD and ebCMOS have similar accuracy and that the ebCMOS shows a better behavior at high noise

levels. We'll see a more detailed comparison of this two detectors in a section below.

4.3.2 Pixel Size

The pixel size is an important parameter in a detector, because it gives an important limit on its accuracy. The first assumption is that the more the pixel is small the more accurate we can be. It is not a completely false assumption but we have to take into account several issues. First of all a smaller pixel size means a bigger number of pixels and then a longer acquisition time to read the same area. The second problem is that a smaller pixel collects less photons but still have the same readout noise. Thus the noise becomes more and more important, to the point where it overcomes the signal. In Fig. 9 the limit of the localization is plotted as a function of the pixel size for the three types of devices.

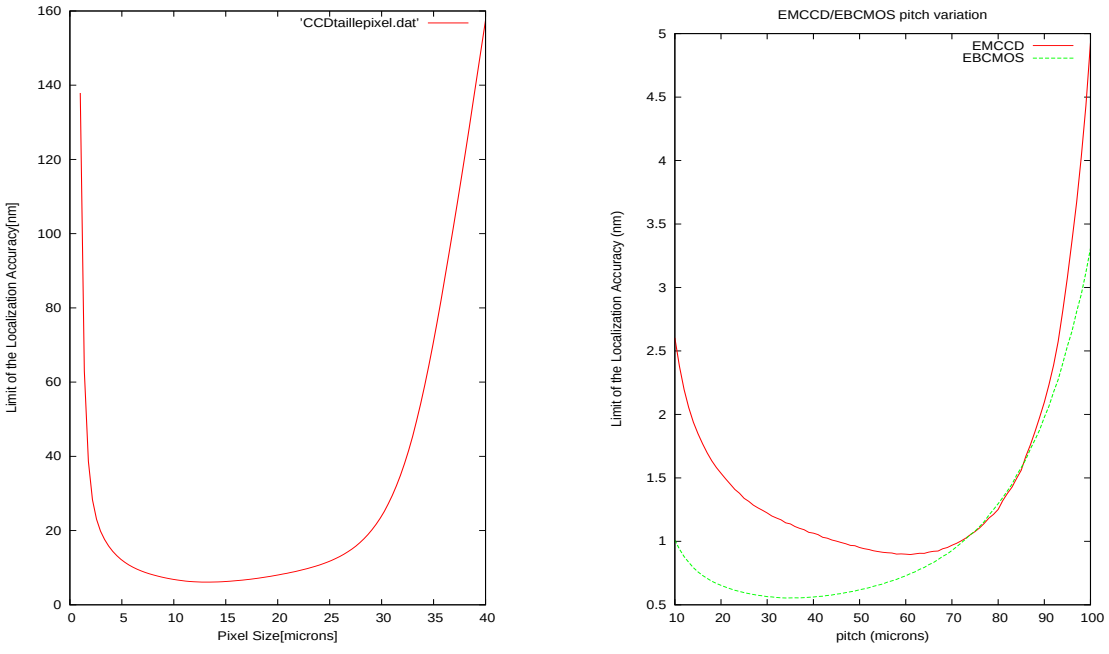

Figure 9: Pixel size variation for CCD (left) and EMCCD and ebCMOS (right).

We can see the same behavior with the EMCCD and ebCMOS but the gain process allows a larger pixel size. It takes into account even photons

far from the center of the source and then even a few large pixel can fit the position when these photons would have been drawn in the readout noise for the CCD. Moreover we see that the minimum is flat thus the choice of the pixel size is relatively free around the minimum (± 5 μm).

4.3.3 Source Position

The position of the source also changes the limit of the accuracy for a simple reason. If the source is in the center of a pixel, then most of the photons will go through this pixel and the main to fit information is given by this pixel. But if the source is placed between two pixels then a better accuracy of the position is obtained. In Fig. 10 the ratio of the limit of localization to the minimum localization is plotted as a function of the position of the source in a pixel (0 is the center, 1 and -1 are the ends) for the three devices.

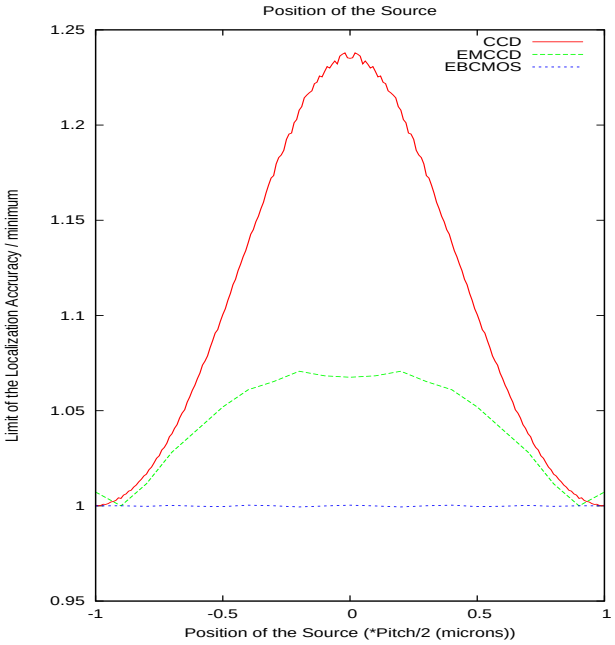

Figure 10: Position Source Variations

The CCD is very sensitive to that (up to 25%). The EMCCD fit more pixels thanks to the gain then the effect is less important but still here (more than 5%). The ebCMOS is flat due to its gain process and the cmos spreading of the created electrons (see Fig. 4).

4.4 CCD and EMCCD Comparison

We now compare CCD detectors with an EMCCD detector to see the gain contribution to the localization accuracy.

4.4.1 Readout noise

Readout noise is the problem of CCD at low signal. That's why the gain process is so important. In Fig. 11 we plotted first the limit of localization accuracy as a function of the number of detected photons for CCD for different readout noises then as a function of the readout noise at fixed signal.

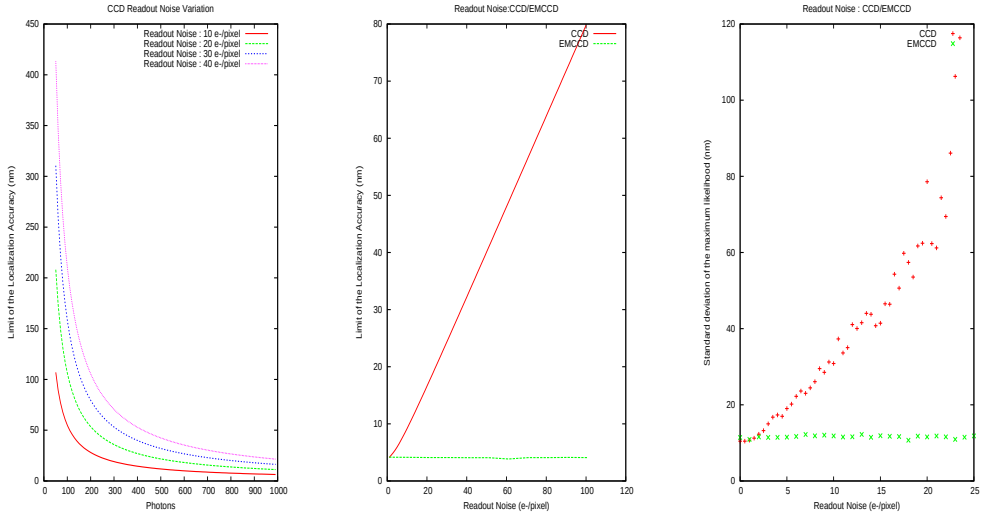

Figure 11: Readout Noise Variations for CCD detectors (left),Readout Noise Variations for CCD and EMCCD detectors using the Cramer Rao Limit (middle) and the Monte Carlo Simulation (right)

This is where the gain stage shows its potential. With the gain stage the detected signal is multiplied by a thousand so that the readout noise becomes negligeable. Then the readout noise shows no effect on the EMCCD when it decreases the accuracy dramatically for the CCD.

4.4.2 Scattering Noise

The drawback of the EMCCD gain stage is that scattering photon noise are also amplified. And because of the nonlinearity of the gain, a scattering

photon could create more charge on the output than a photon from the source. In Fig. 12 the limit of localization accuracy is plotted as a function of the scattering noise for CCD and EMCCD.

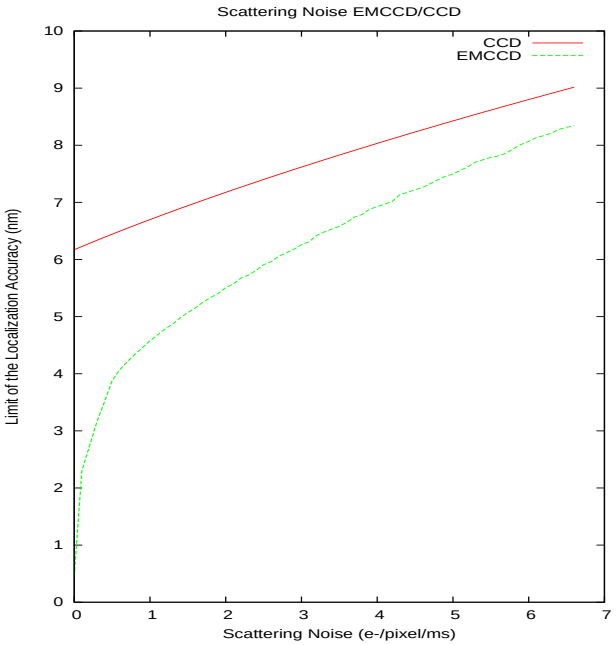

Figure 12: Scattering Noise Variations for CCD and EMCCD detectors

We can see that the effect of scattering noise is very important for EMCCD with the steep slope when the scattering noise is turned on.

4.5 ebCMOS

The ebCMOS detector has two new psf stages: the tube and the cmos stages. Each has a certain p.d.f. that can be changed. In Fig. 13 the variation of the ML is plotted as a function of the variance of the different psf.

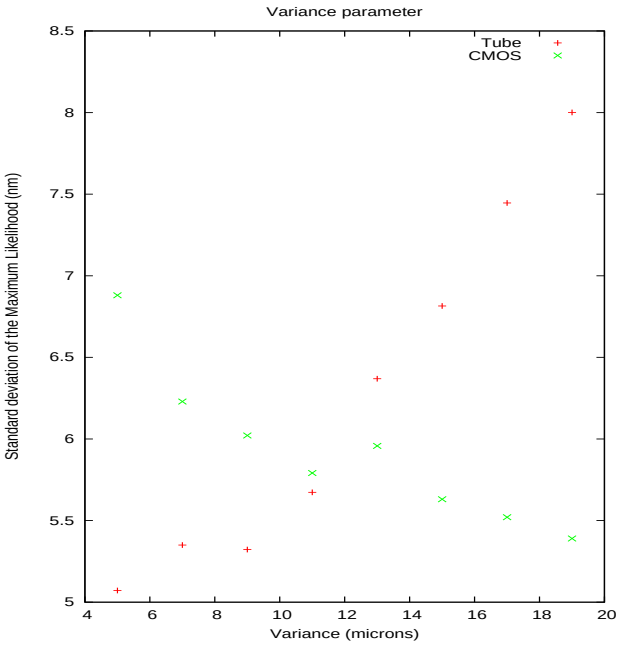

Figure 13: variance of pdf

As we can see, the tube stage behaves as expected, when it spreads the photons, the precision descreases. But the cmos stage behaves in the opposite way. If everything is in the same pixel (small σ_{cmos}, we have a precision of only a pixel (binary resolution). If it spreads to several, we can fit the position and achieve an intra pixel accuracy.

4.6 EMCCD ebCMOS Comparison

We can try to compare the two gain processes to each other using their best current features to see wichever is best at a certain number of emitted photons. In Fig. 14 the variation of the ML is plotted as a function of the number of emitted photons for the EMCCD and the ebCMOS for different QE.

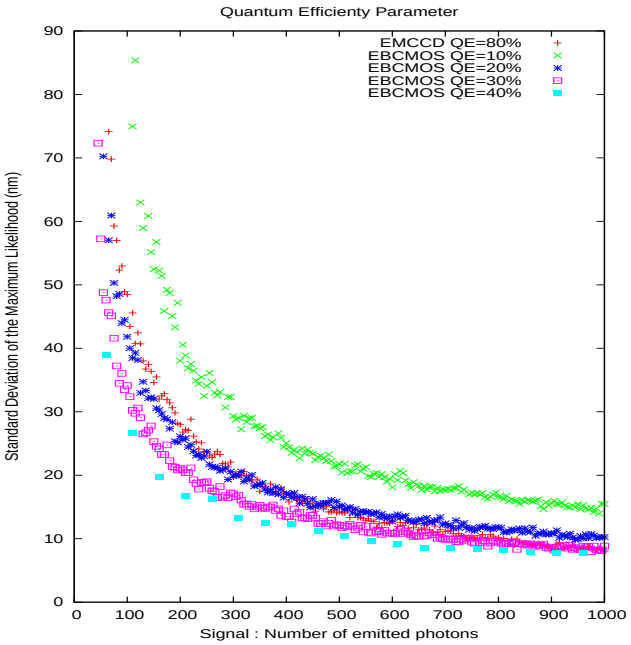

Figure 14: ML vs number of emitted photon for different QE

The current generation of detector used in our group has a 15% QE but 30% to 40% is expected for the new generation thus it is fair to notice that the ebCMOS shows a better accuracy at low signal and that the EMCCD is better around 1000 emitted photons per frame.

5 Summary and Prospects

5.1 Summary

We saw in this study that a gain stage is necessary when the signal decrease, EMCCD and ebCMOS allows the same accuracy than a CCD with 10 to 100 times less photons: around 40 nm with 100 photons per frame. Moreover the two gain processes show equivalent intrinsic accuracy for an ebCMOS with good QE. Besides, for a deeper understanding we also have to take into account the processing authorized by this new type of detector.

5.2 Acquisition Time and Processing

In this work we voluntarily forgot another main difference between EMCCD and ebCMOS, the acquisition time: around 30 ms or 33 fps for EMCCD and 2ms or up to 500 fps for ebCMOS. We didn't take it into account because it goes beyond the sheer capacity of the detectors to the processing. That should be a great advantage for ebCMOS according to the good resolution at low signal. Indeed each frame has less photons but if only a couple a them touch the detector then it is enough to follow the emitting source and accumulate signal photons to obtain the sufficient number of detected photon for the expected accuracy. At each frame we can use the datas from previous frames and compute an expected position of the target taking into account the spatial pdf. This method allows an online visulaization of the detected target with an increasing localization accuracy up to the resolution required by the user or to the bleaching of the source. One of the most robust method is called a Kalman filter. The Monte Carlo of this work has been used in our group to test and improve the Kalman filter implementation of our camera software acquisition.

Moreover this allows us to follow a moving source [19, 20] and if the signal is strong enough allows a better fit on the localization of the source. If the source moves during the acquisition time then the best measure of its size is the difference between the starting point and the endpoint. Thus with an acquisition time 15 times less, although we would lose accuracy, we could expect to follow a mouvement such as the brownian movement.

5.3 Photon Counting

In this work we also skipped another use of the detectors: the photon counting from one to five photons in the same cluster. Thanks to its linear gain, the ebCMOS is capable of counting the exact number of photons detected in the same cluster and to give their position as shown in the Fig. 15. That could bring new possibilities in the implementation of ultra fast online target tracking based on exact photon counting and localization.

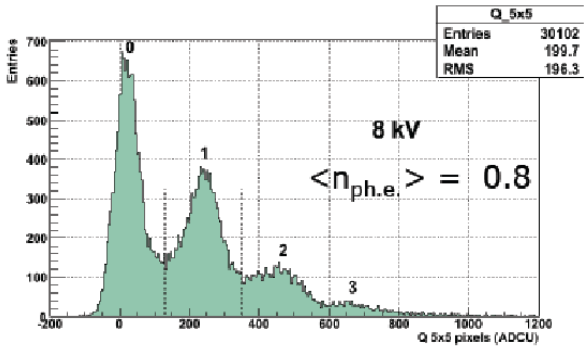

Figure 15: Photon Counting

References

[1] Russel E. Thompson, Daniel R. Larson, and Watt W. Webb. Precise Nanometer Localization Analysis for Individual Fluorescent Probes. *Biophysical Journal*, 82:2755–2783, 2002.

[2] Samuel T. Hess, Thanu P. K. Girirajan, and Michael D. Mason. Ultra-High Resolution Imaging by Fluorescence Photoactivation Localization Microscopy. *Biophysical Journal*, 91:4258–4272, 2006.

[3] Eric Betzig, George H. Patterson, Rachid Sougrat, O. Wolf Lindwasser, Scott Olenych, Juan S. Bonifacino, Michael W. Davidson, Jennifer Lippincott-Schwartz, and Harald F. Hess. Imaging Intracellular Fluorescent Proteins at Nanometer Resolution. *Science*, 313:1642–1645, 2006.

[4] Hari Shroff, Helen White, and Eric Betzig. Photoactivated Localization Microscopy (PALM) of Adhesion Complexes. *Wiley Interscience*, 41, 2008.

[5] Fabien Pinaud and Maxime Dahan. Zooming Into Live Cells. *Science Magazine*, 320:187–188, 2008.

[6] Rainmund J. Ober, Sripad Ram, and E. Sally Ward. Localization Accuracy in Single-Molecule Microscopy. *Biophysical Journal*, 86:1185–1200, 2004.

[7] Donald L. Snyder and Abed M. Hammoud. Image Recovery from Data Acquired with a Charge-Coupled-Device Camera. *Journal of the Optical Society of America A*, 10:1014–1023, 1993.

[8] Michael J. DeWeert, Jeffrey B. Cole, Andrew W. Sparks, and Andrew Acker. Photon Transfer Methods and Results For Electron Multiplication CCDs. *Applications of Digital Image Processing XXVII*, 5558:248–259, 2004.

[9] R. N. Tubbs. *Lucky Exposures: Diffraction Limited Astronomical Imaging Through the Atmosphere*. 2003.

[10] Olivier Daigle, Claude Carignan, and Sebastien Blais-Ouellette. Faint Flux Performance of an EMCCD. *Online Publication*, 2006.

[11] Mark Stanford Robbins and Benjamin James Hadwen. The Noise Performance of Electron Multiplying Charge-Coupled Devices. *IEEE Transactions on Electron Devices*, 50:1227–1232, 2003.

[12] Colin Coates, Boyd Fowler, and Gerhard Holst. sCMOS White Paper. , 2009.

[13] Guy Meynants, Bart Dierickx, and Danny Scheffer. CMOS Active Pixel Image Sensor with CCD Performance. *SPIE/EUROPTO AFPAEC Conference*, 1998.

[14] Boyd Fowler and Xinqiao (Chiao) Liu. Charge Transfer Noise in Image Sensors. *International Image Sensor Workshop*, 2007.

[15] Donald L. Snyder, Carl W. Helstrom, Aaron D. Lanterman, Mohammad Faisal, and Richard L. White. Compensation for Readout Noise in CCD Images. *Journal of the Optical Society of America A*, 12:272–283, 1995.

[16] R. Barbier, P. Depasse, J. Baudot, W. Dulinski, M. Winter, N. Estre, N. Laurent, C.T. Kaiser, and S. Katsanevas. First results from the development of a new generation of Hybrid Photon Detectors : EBCMOS. *International Conference on Advanced Technology and Particle Physics*, 2007.

[17] W. J. Metzger. *Statistical Methods in Data Analysis*. NIJMEGEN, 2006.

[18] Adam Merberg and Steven J. Miller. Course Notes for Math 162: Mathematical Statistics: The Cramer-Rao Inequality. , 2008.

[19] Sebastien Courty, Camilla Luccardini, Yohanns Bellaiche, Giovanni Cappello, and Maxime Dahan. Tracking Individual Kinesin Motors in Living Cells Using Single Quantum-Dot Imaging. *Nano Letters*, 6:1491–1495, 2006.

[20] Maxime Dahan, Sabine Levi, Camilla Luccardini, Philippe Rostaing, Beatrice Riveau, and Antoine Triller. Diffusion Dynamics of Glycine Receptors Revealed by Single-Quantum Dot Tracking. *Science*, 302:442–445, 2003.